A proxy for determining solar wind dynamic pressure at Mars using Mars Global Surveyor data

Dana H. Crider,[1] Didier Vignes,[2] Alexander M. Krymskii,[3] Tamara K. Breus,[4] Norman F. Ness,[5] David L. Mitchell,[6] James A. Slavin,[2] and Mario H. Acuña[2]

Received 31 January 2003; revised 6 September 2003; accepted 7 October 2003; published 31 December 2003.

[1] We develop a method to infer the upstream solar wind pressure at Mars using data from the Mars Global Surveyor (MGS) magnetometer instrument. The method assumes magnetic field pressure in the magnetic pileup region balances the incident solar wind dynamic pressure. Newtonian pressure balance conditions are imposed for positions off of the subflow point. Proof of concept exists from the mapping phase of the spacecraft mission, when the orbital geometry at a constant altitude allows fits to magnetic field data as a function of solar zenith angle. During the elliptical orbit phase of MGS, when the spacecraft passes through a large range of altitudes, such fits are not possible. However, the measured magnetic pressure in the magnetic pileup region is scaled by the same means as derived for the mapping orbits and reasonable upstream solar wind pressure is obtained. We compare the distribution of solar wind pressure calculated using MGS data with the solar wind pressure measured upstream of the Earth during the same time period and find good agreement, further supporting this algorithm as a valid proxy for the incident solar wind pressure. The response of the position of the Magnetic Pileup Boundary to the inferred solar wind pressure also validates the method. High solar wind ram pressure depresses the altitude of the Magnetic Pileup Boundary. *INDEX TERMS:* 2780 Magnetospheric Physics: Solar wind interactions with unmagnetized bodies; 2756 Magnetospheric Physics: Planetary magnetospheres (5443, 5737, 6030); 5421 Planetology: Solid Surface Planets: Interactions with particles and fields; 5494 Planetology: Solid Surface Planets: Instruments and techniques; 6225 Planetology: Solar System Objects: Mars; *KEYWORDS:* solar wind dynamic pressure, Mars Global Surveyor, magnetic pileup boundary, magnetic pileup region, Venus magnetic barrier

Citation: Crider, D. H., D. Vignes, A. M. Krymskii, T. K. Breus, N. F. Ness, D. L. Mitchell, J. A. Slavin, and M. Acuña, A proxy for determining solar wind dynamic pressure at Mars using Mars Global Surveyor data, *J. Geophys. Res.*, *108*(A12), 1461, doi:10.1029/2003JA009875, 2003.

1. Introduction

[2] The solar wind interaction with planetary bodies is modulated by the incident solar wind pressure. For example, as solar wind pressure fluctuates, the Earth's magnetopause responds by moving in and out [*Sibeck et al.*, 1991]. Other examples of properties governed by the incident solar wind pressure include the magnetization of the ionosphere of Venus [*Luhmann et al.*, 1980] and the diameter of the martian magnetotail cavity [*Dubinin et al.*, 1996]. Because it drives many important processes, it is essential to know the incident solar wind pressure for studies of the solar wind interaction with a planet.

[3] Previous research on the solar wind interaction with Mars utilized the plasma data available from the early Soviet Mars spacecraft and the Phobos-2 spacecraft. From these missions, *Schwingenschuh et al.* [1992] found that the Martian bow shock does not respond to changes in solar wind pressure, like Venus [*Slavin et al.*, 1980]. In contrast, the bow shock from a magnetospheric obstacle to the solar wind does move with solar wind pressure. The difference in the two situations is that the obstacle size changes significantly in the magnetospheric case, whereas it does not change much in the ionospheric obstacle (Venus-like) case.

[4] In the tail of Mars, Phobos-2 data suggested a solar wind pressure dependence on the width of the tail cavity [*Verigin et al.*, 1993]. The tail width to the inverse sixth power was proportional to P_{sw}. Such a response was interpreted as evidence for an intrinsic magnetic field at Mars. Mars Global Surveyor data has since shown that a significant intrinsic dipole does not exist at Mars [*Acuña et al.*, 1998]. However, there are regions of remanent mag-

[1]Department of Physics, Catholic University of America, Washington, DC, USA.
[2]NASA Goddard Space Flight Center, Greenbelt, Maryland, USA.
[3]Rostov State University, Rostov-on-Don, Russia.
[4]Space Research Institute, Moscow, Russia.
[5]Bartol Research Institute, University of Delaware, Newark, Delaware, USA.
[6]Space Science Laboratory, University of California, Berkeley, California, USA.

0148-0227/03/2003JA009875

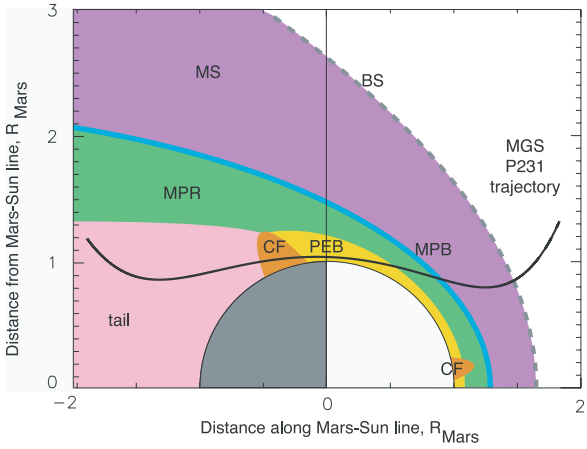

Figure 1. Cylindrical projection of the trajectory of MGS pass 231 to show the locations of the different regimes. The shaded areas represent the bow shock (dashed line), magnetosheath (purple), MPB (blue), magnetic pileup region (green), photoelectron boundary (yellow), a crustal field (orange), and the tail (pink) (see Figure 2).

netization in the Martian crust [*Acuña et al.*, 1998]. Current research is trying to determine the amount of influence the remanent fields have on the solar wind interaction with Mars [see *Brain*, 2002; *Crider*, 2003].

[5] Despite these interesting results, there remained many open issues regarding the solar wind interaction with Mars following the Phobos-2 mission. The spatial coverage of Phobos-2 was limited. The spacecraft closest approach was 860 km altitude. Further, all but the first five orbits were circular, equatorial orbits. Much of the Martian ionosphere and dayside magnetosheath was unexplored by comprehensive plasma experiments packages.

[6] The orbit of the Mars Global Surveyor (MGS) spacecraft during the aerobraking phase of the mission was ideal for examining aspects of the solar wind interaction with Mars. MGS is equipped with a magnetic fields experiment that includes two magnetometers and electron reflectometer (MAG/ER), providing vector magnetic fields data and electron fluxes from 10 eV to 20 keV energy [*Acuña et al.*, 1992]. Unlike previous spacecraft at Mars, MGS routinely dipped below the martian ionosphere. Its elliptical orbit also carried the spacecraft out into the preshocked solar wind. (For a detailed account of MGS orbital coverage, see *Albee et al.* [2001] and *Brain et al.* [2002].) Despite the excellent orbital coverage for studying the solar wind interaction with Mars, no ion instrument is on board to provide simultaneous ion data for analysis with magnetic field data. Therefore it is impossible to directly measure the solar wind pressure with MGS instrumentation. In order to maximize the information gained from the MGS data, we develop a proxy to estimate the upstream solar wind pressure in this paper.

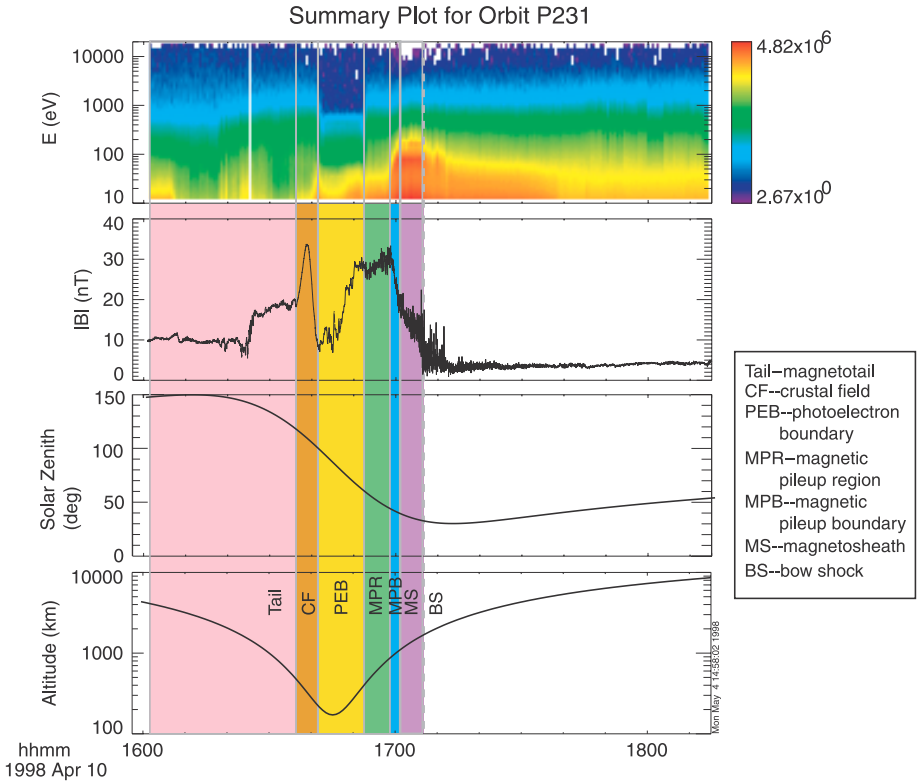

Figure 2. Time series data from periapsis pass 231 on 10 April 1998. The panels from top to bottom display electron fluxes, magnetic field magnitude, solar zenith angle, and spacecraft altitude. The shaded areas represent from right to left the bow shock (dashed line), magnetosheath (purple), MPB (blue), magnetic pileup region (green), photoelectron boundary (yellow), a crustal field (orange), and the tail (pink). The color codes correspond to the regions in Figure 1.

[7] In section 2, we discuss the pressure balance throughout the interaction region and the basis for determining the upstream solar wind pressure. Then, in section 3, we develop the proxy for solar wind pressure for use with MGS data. In section 4, we show techniques to validate the proxy. Finally, in section 5, we look at the response of the Martian magnetic pileup boundary to the inferred solar wind pressure.

2. Solar Wind Interaction With Mars

[8] There is pressure balance throughout the region of solar wind interaction with Mars assuming steady state conditions. The dominant component of the pressure changes according to local conditions, but the total pressure anywhere in the interaction region is equal to the incident pressure, p_{sw}. Although MGS does not measure p_{sw}, we can determine the total pressure incident on the planet by analogy if we know the total pressure at another point. For this purpose, it is instructive to divide the area around Mars into regions based on the characteristics of the plasma and the dominant pressure component. These regimes are illustrated in Figure 1 and discussed below.

[9] Figure 1 gives the cylindrical half-plane projection of Mars. The planet is approximated by a half-circle. The Sun is to the right. Also shown are fits to the well-known boundaries in the solar wind interaction with Mars: the Bow Shock (BS) and the Magnetic Pileup Boundary (MPB) [*Vignes et al.*, 2000]. The mean BS location is represented by the gray dashed line. The MPB is the blue line in Figure 1.

[10] Figure 2 is the time series MAG/ER data from a periapsis pass around Mars on 10 April 1998. It was MGS orbit 231. The spacecraft trajectory is shown on Figure 1 and the color codes are the same in Figures 1 and 2 for ease of comparison. The top panel is the electron spectrogram, giving electron fluxes as a function of energy and time. The next panel is the magnetic field magnitude. The bottom two panels display the position of MGS (solar zenith angle and altitude) as a function of time.

[11] Upstream of the planet is the free-flowing solar wind (white region in Figure 1). Here p_{sw} is dominated by the ram pressure term, ρv^2, where ρ is the mass density of the plasma and v is the flow velocity. In general at planetary bow shocks, the solar wind plasma is compressed, heated, and slowed, while the magnetic field magnitude jumps. The thermal pressure term, p_t, increases while ρv^2 decreases. Thermal pressure is important throughout the magnetosheath, which exists between the BS and MPB and is the region colored purple in Figures 1 and 2. The martian magnetosheath is characterized by turbulent magnetic fields [*Cloutier et al.*, 1999] (see Figure 2) and the presence of solar wind protons [*Rosenbauer et al.*, 1989; *Lundin et al.*, 1989].

[12] The Magnetic Pileup Boundary (MPB) is the boundary between magnetosheath plasma and the region of piled-up magnetic field. The MPB is apparent in MGS data as an increase in magnetic field magnitude accompanied by a simultaneous decrease in electron fluxes over an altitude of a few 10 to a few 100 km [*Acuña et al.*, 1998; *Vignes et al.*, 2000] as shown in Figure 2 in blue. Instruments on Phobos-2 detected a shift in ion composition from solar wind protons to heavy ions presumably of planetary origin at a position named the Ion Composition Boundary [*Breus et al.*, 1991]. The change in plasma composition suggests that the solar wind ions are deflected at this boundary. It is coincident with the MPB [*Trotignon et al.*, 1996; *Vignes et al.*, 2000]. The location of the MPB is highly variable and appears to respond to the influence of crustal magnetic fields [*Crider et al.*, 2002] and solar wind pressure [*Verigin et al.*, 1993].

[13] Below the MPB is the Magnetic Pileup Region (MPR). This region is several hundred km thick and is shown in green in Figure 1. MGS data confirms that the MPR consists of IMF flux tubes that are draped around the planet [*Bertucci et al.*, 2003; *Brain et al.*, 2003; *Crider et al.*, 2003]. The plasma in the MPR appears to comprise cooled electrons [*Crider et al.*, 2000] and heavy ions [*Rosenbauer et al.*, 1989; *Lundin et al.*, 1989]. The signatures of this region indicate the planetary exosphere plays a major role in its formation [*Crider et al.*, 2000; *Chen et al.*, 2001]. Theory predicts that at the nose of the planet, the flow slows to a halt and plasma is squeezed out of the magnetic field lines by the *Zwan and Wolf* [1976] effect. The pressure there is dominated by magnetic field pressure, $B^2/2\mu_o$ [*Øieroset et al.*, 2003].

[14] Below the MPR, there is a region in which the electron signature changes [*Mitchell et al.*, 2000]. The region in yellow in Figure 1 is termed the photoelectron boundary (PEB) because it is the region in which the 10 eV to 20 keV electron fluxes are dominated by locally produced photoelectrons. In Figure 2, one can see the decrease in electron fluxes, especially at energies greater than 200 eV. Above the PEB, cooled solar wind electrons on the magnetic field lines overwhelm the signal from photoelectrons. The ''appearance'' of photoelectrons below the MPR indicate that solar wind electrons do not have access to that region [*Mitchell et al.*, 2000]. Because electrons are closely bound to magnetic field lines, the PEB demarks the region in which the magnetic field lines no longer have access to the solar wind.

[15] Scattered within the martian crust are regions of intense magnetization [*Acuña et al.*, 1998]. These magnetic anomalies are highly localized and concentrated in the southern hemisphere of the planet between 140° and 240° W. longitude [*Acuña et al.*, 1999; *Connerney et al.*, 2001]. They are represented by orange bumps in Figure 1. Crustal magnetic fields affect the environment to altitudes of up to 1300 km in places [*Brain et al.*, 2003]. Usually, crustal fields protrude into the PEB and MPR areas. There is some evidence that the presence of crustal fields raise the MPB to higher altitudes [*Crider et al.*, 2002]. There is no evidence that the magnetic field of the anomalies extend into the magnetosheath other than raising the minimum sheath altitude, the MPB. The bow shock location does not seem to be modulated by crustal fields or subsolar longitude [*Vignes et al.*, 2002; *Slavin et al.*, 1991].

[16] For nonmagnetic obstacles, the magnetotail comprises IMF lines draped around the planet. It is the region behind the planet represented by pink in Figures 1 and 2. Phobos-2 spent a lot of time in the martian magnetotail due to its orbit at 9600 km. *Lundin et al.* [1990] detected the outflow of O^+ ions in the magnetotail. Recent data from MGS suggest that it is possible that the magnetic field from

the crustal fields leak into the martian magnetotail [*Krymskii et al.*, 2002].

3. Pressure Determination

[17] MGS does not measure thermal pressure or ram pressure but can determine magnetic pressure along its orbital trajectory. In order to deduce the incident solar wind dynamic pressure on Mars, we focus on a region in which magnetic pressure dominates. The crustal fields are such regions; however, we can not use them for this purpose. In fact, data taken near regions of high crustal magnetization are avoided. Regions above crustal sources contain magnetic field from both the interplanetary magnetic field and the crustal sources. Only the contribution from magnetic fields associated with currents generated by the solar wind interaction are of importance. The contribution from the planet cannot easily be isolated and removed from the total field measured. Further, they are localized in nature and constantly change orientation with respect to the IMF as the planet rotates and the IMF fluctuates. Reconnection can occur [*Brain*, 2002]. Therefore they are not always in steady state.

[18] In the PEB, magnetic field remains high for some distance (see yellow region in Figure 2), but ionospheric thermal pressure begins to dominate. Data indicate that this region is not in steady state, as the boundary moves up and down in time in response to several factors [*Mitchell et al.*, 2001]. Also, crustal fields are more likely to contribute to the magnetic field measurements in the PEB [*Crider et al.*, 2001]. Instead, we focus on the magnetic field in the MPR for inferring the upstream solar wind pressure.

[19] Inspection of Figure 2 reveals that the magnetic field magnitude is high throughout the MPR. Magnetic pressure seems to dominate in the MPR and that pressure is derived from the solar wind. Apparently, the MPB is a boundary for solar wind protons [*Lundin et al.*, 1989], but the interplanetary magnetic field is carried through into the PEB. (Although magnetic fields originating in the crust of Mars are present in some localized regions [*Acuña et al.*, 1998], there are many regions below the MPB in which the magnetic field is primarily draped IMF flux tubes [*Brain et al.*, 2003; *Crider et al.*, 2003].) MGS data indicate that the MPR consists of evacuated IMF flux tubes and thus low thermal pressure [*Øieroset et al.*, 2003].

[20] In this work, we assume that the MPR is the transition between solar wind dominated plasma and planetary dominated plasma analogous to the transition region at Venus [*Zhang et al.*, 1991]. At Mars, the transition has a different appearance than at Venus. The pileup of magnetic field occurs over a very short altitude at Mars (several 10s to a few hundred km) compared with at Venus (several hundred km). At Mars, the piled-up magnetic field remains high for several hundred km. In contrast, the magnetic field builds up gradually at Venus, attaining the peak value close to the bottom of the magnetic barrier before steeply dropping off in the ionosphere. These differences are intriguing. Understanding the reasons for the different behavior of the magnetic field at the two objects will certainly unravel important physics involved in the formation of the regions.

[21] At the stagnation point, one can equate the measured magnetic pressure to p_{sw} if the thermal pressure is negligible. However, MGS does not pass through the stagnation point along its trajectory. Away from the subflow line, the flow has components parallel to the obstacle. One must account for the curvature of the obstacle by having the incident pressure drop with the angle between the ram direction and the surface normal, θ. In solar wind interactions, it has been found that the Newtonian pressure balance accurately describes the pressure drop due to the curvature of the obstacle [see, e.g., *Spreiter and Stahara*, 1992]:

$$p_{obstacle} \propto p_{incident} \cos^2 \theta. \quad (1)$$

The pressure at the obstacle is the sum of magnetic pressure and thermal pressure. Apart from a proportionality constant, k, we then have a proxy for the upstream solar wind pressure, p_{sw}:

$$k p_{sw} \cos^2 \theta = B^2/2\mu_o + p_t \quad (2)$$

Typical values of k are around 0.88.

[22] What then is the obstacle surface in the case of Mars? For this work, we assume the solar wind obstacle has the shape of the Magnetic Pileup Boundary (MPB). Because the MPB appears to be the obstacle to solar wind protons, it is logical to use it to derive the obstacle shape. We use the conic section best fit to the MGS MPB crossings [*Vignes et al.*, 2000] to provide the normal to the obstacle surface as a function of solar zenith angle. Figure 3 shows the average

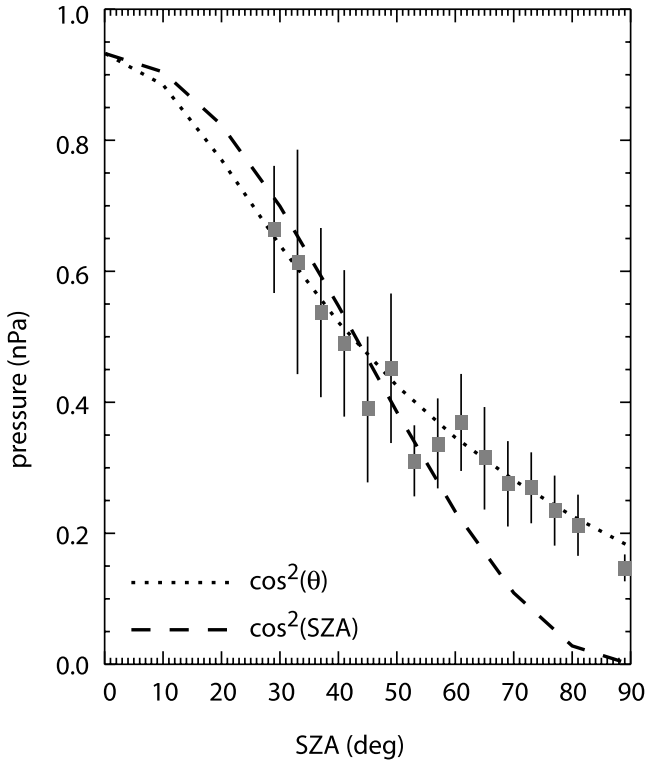

Figure 3. The plot shows the pressure as a function of solar zenith angle. Averages by 4 degree bins (squares) and ±1 standard deviation bars use only points with inferred solar wind pressure in the middle two quarters of the distribution. The solid (dashed) line superimposes the fits of $\cos^2 \theta$ ($\cos^2$SZA).

and ±1σ bars of the local magnetic pressure for data in 4° SZA bins. Fits using equation (2) with two different obstacle shapes are also shown in Figure 3. Inspection reveals that equation (2) fits the data much better using the MPB shape than using a hemispherical obstacle shape. Further, a residual solar zenith angle dependence remained in the data using a hemispheric obstacle, indicating that the obstacle is not a simple hemisphere (see also section 4.1). Alternatively, *Verigin et al.* [2003] have used the minimum variance direction of the magnetic field to determine the obstacle shape. *Zhang et al.* [1991] have used a polynomial fit to the peak magnetic field height for the obstacle shape at Venus.

[23] We measure the magnetic field in the magnetic pileup region on each MGS dayside pass to determine $B^2/2\mu_o$. It is appropriate to consider only the magnetic field parallel to the obstacle boundary [*Verigin et al.*, 1993]. However, *Bertucci et al.* [2003] have found that the magnetic field is predominately parallel to the obstacle boundary inside of the MPR. It is important to remember that the Martian obstacle is "bumpy" because of the presence of crustal fields [*Crider et al.*, 2002; *Brain*, 2002]. We do not use only the parallel component of magnetic field in this work because it would compound any error in the assumed obstacle shape. This choice is supported by the good results *Verigin et al.* [2003] have achieved in assuming the magnetic field is parallel to the obstacle boundary using these data.

[24] This method assumes that the contribution from gas pressure is small and therefore p_t is neglected. Thus the inferred solar wind pressure, p_{MGS}, is:

$$p_{MGS} = \frac{B_{MPR}^2}{2\mu_o k \cos^2\theta}. \quad (3)$$

This is a reasonable assumption upstream of the planet and at high solar zenith angles where the flow is supersonic. It is also reasonable in the MPR at low solar zenith angles where magnetic pile-up is a maximum. In Figure 3 we fit the data to equation (2) using a χ^2-minimizing fit to the linearized version of the function. The best fit values are $kp_{sw} = 0.932$ nPa and $p_t = 0.004$ nPa. For $k = 0.88$, the thermal pressure in the MPR is 0.4% of the average solar wind pressure (p_{sw} = 1.06 nPa). This is much lower than p_t at Venus, which could reach 33% of the upstream pressure [*Vaisberg et al.*, 1980]. Although confirmation by ion measurements in the MPR would be helpful, our analysis suggests the thermal pressure in the MPR is insignificant. This is not surprising given the sparse plasmas at Mars. *Øieroset et al.* [2003] have used MGS electron fluxes to derive electron temperature and density in the MPB and MPR for two MGS orbits. Their results produce electron thermal pressures in agreement with our value. Even if the ion thermal pressure is more than a factor of 10 greater, p_t is only a small component in the MPR.

[25] This proxy is intended for intracomparison of data from different MGS orbits. Any comparison using relative solar wind pressures derived via this method are accurate. Absolute values for pressure can be determined using equation (2) and an estimate of p_t. We point out that if the thermal pressure were actually much higher than our analysis suggests, it would not affect the relative values on the solar wind pressure much. Calculations with thermal pressure set to 0.1 nPa (approximately 10% of the average solar wind pressure) had little effect on the relative distribution of inferred p_{sw}. However, to compare to solar wind pressure measured by Phobos-2, for example, it is recommended that the data sets be compared as a whole and renormalized. In fact, because solar wind pressure varies throughout the solar cycle, we recommend the consideration of p_{sw} measured at Earth for the two epochs in the renormalization. Otherwise, a one-to-one comparison of absolute values between data sets is not recommended.

4. Validation of Method

4.1. Selection Effects

[26] When selecting data, one risks introducing biases into the results. We checked the proxy for systematic biases by looking at the inferred solar wind pressure as a function of several parameters.

[27] The MPR is a thick region. MGS takes several hundred vector magnetic field measurements within the MPR on each orbit. The points used to determine the upstream pressure are chosen by the longest unbroken stretch within the MPR that met three selection criteria. First, we use data that have low variability. This removes data contaminated by waves or unsteady conditions. Second, we choose only data remote from known crustal sources. This is achieved by omitting data from areographic latitude and longitude that have an average field from the mapping orbits exceeding 10 nT in the *Connerney et al.* [2001] analysis. Finally, we use only data obtained at $\theta < 75°$. Because equation (3) has a $\cos^2\theta$ factor in the denominator, the expression begins to blow up at larger θ. The magnetic field vectors were averaged over the height of the longest continuous segment to a maximum 100 km altitude change.

[28] Upon comparing several data selection methods, we obtain similar relative values using data from anywhere within the MPR so long as crustal sources were avoided. The result is independent of the altitude of the measurement as long as it was from within the MPR. No dependence on the angle of the measurement was found for $\theta \leq 75°$. Even when altering the selection criteria to use the peak magnetic field or the magnetic field at a specific altitude, for example, the results do not change significantly. Therefore Newtonian approximation appears to be accurate. Likewise, the choice of obstacle shape is valid. Finally, equation (3) using magnetic field within the MPR is an appropriate proxy for p_{sw}.

4.2. External Influences

[29] Next, we look for a temporal dependence of p_{sw}. There are real periodicities in p_{sw}. For example, p_{sw} varies slightly with the solar cycle with p_{sw} at a minimum near solar maximum [*Diodato et al.*, 1974]. This study derives from a short segment of the solar cycle, so this effect is expected to be minimal.

[30] Also, the density of the solar wind falls with $1/r^2$. Therefore the slight eccentricity of Mars' orbit around the Sun will impose higher pressure a perihelion. The peak to trough change in pressure from this is 19%. The measurements are from a significant fraction of the Martian year.

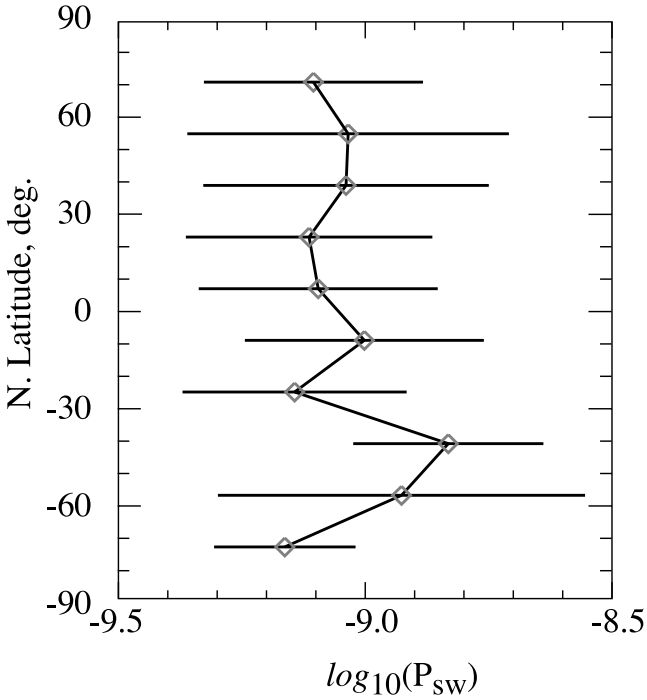

Figure 4. Average (diamonds) and ±σ (error bars) of the log pressure binned by the latitude of the measurement in planetocentric coordinates.

[31] Martian seasonal effects could influence p_{MGS}. One can imagine that the martian magnetic field topology varies with subsolar latitude. In northern hemisphere summer, the strongest crustal fields, which are in the southern hemisphere, are tilted further away from the subsolar point on the planetary dayside. The residual field will stand up higher because there is less pressure compressing the field at those high angles. So it is easy to imagine that magnetic field magnitudes in the MPR near crustal sources could be higher during northern summer/southern winter. However, this does not reflect a change p_{sw}. The signal is greatest close to anomalies and at low altitudes. Since the proxy method relies on the magnetic field close to the planet, this must be taken into consideration. No such temporal dependence is evident in the data. Therefore to the level of accuracy here, there are no spurious temporal biases included in the proxy.

[32] The crustal magnetization does influence p_{MGS} in another way. The inferred solar wind pressure taken from points in the 40–60°S latitude band are higher than at other latitudes as shown in Figure 4. These latitudes are the location of very strong crustal magnetization [*Connerney et al.*, 1999; *Acuña et al.*, 2001]. Although the data acquired immediately above known crustal sources was eliminated, the ambient magnetic field magnitude is apparently elevated in that latitude band. The magnetic influence of the crustal sources has slipped into the proxy. However, the effect is not extremely large. Perhaps later revisions of this proxy will only use data in the MPR in the northern hemisphere. However, that would limit the number of orbits for which p_{MGS} can be determined.

[33] Additionally, crustal fields have been shown to displace the position of the magnetic pileup boundary [*Crider et al.*, 2002]. They have such a small scale size that the obstacle shape is significantly distorted from the nominal shape we use by their presence. There, the actual angle of incidence of the solar wind flow on the obstacle is different from the nominal case used in this analysis. Without tailoring the obstacle shape for each individual anomaly, the proxy is invalid near crustal fields. *Verigin et al.* [2003] have considered the magnetic field direction as an estimate of the obstacle surface in their study of the effects of solar wind pressure on the solar wind interaction with Mars.

4.3. Comparison With Wind Data

[34] To further validate our method, we compare p_{MGS} to the measured solar wind pressure upstream of the Earth by the Wind satellite, p_{Wind}. In general, solar wind ram pressure, ρv^2, will drop with the density as r^{-2}, where r is the distance from the Sun. The solar wind velocity does not vary much with distance from the Sun, at least in the Earth-Mars neighborhood. We scale the Wind measurements by the ratio of the distances squared to show the equivalent pressure at 1.5 A.U. (see Figure 5).

[35] Further, solar wind pressure is highly variable and dependent on factors at the origination longitude on the Sun

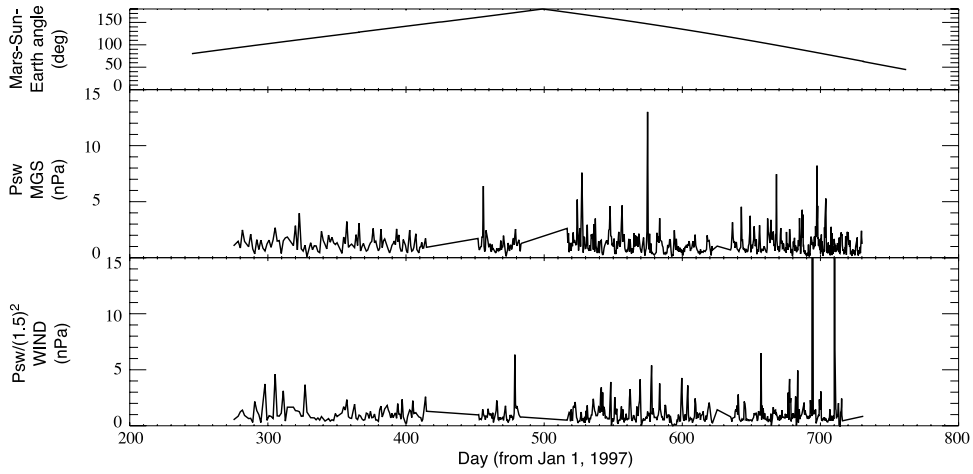

Figure 5. Three panels show as a function of time for the elliptical orbit phase of MGS (from top to bottom) the separation angle between Earth and Mars, the inferred solar wind pressure at Mars from this proxy, and the measured solar wind pressure at Earth by Wind.

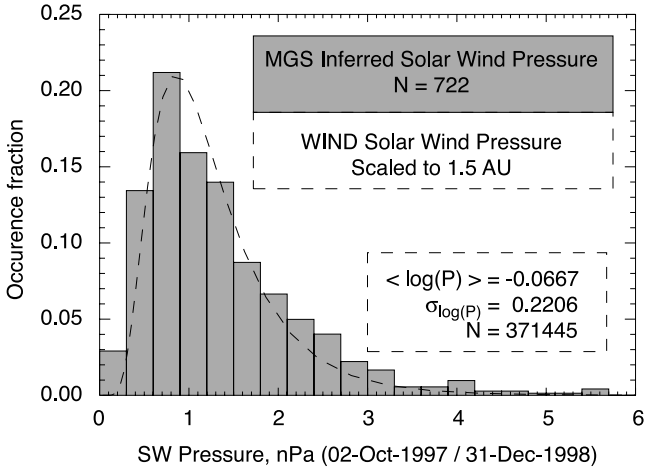

Figure 6. Comparison of the solar wind pressure distribution obtained by this proxy at Mars with the solar wind pressure measured by Wind at Earth during the same time period.

[*Sheeley and Wang*, 1991]. If Mars were at opposition, one might expect similar solar wind conditions at Earth and Mars after adjusting for the transit time for the solar wind from Earth orbit to Mars orbit. A one-to-one correlation is not expected for the solar wind pressure at Earth and at Mars during the elliptical orbit phase. As shown in the top panel of Figure 5, Mars is closer to conjunction than opposition during this time period. Therefore Mars is subjected to conditions at a much different solar longitude at all times. In the ~10 or so days it takes for the same solar longitude to rotate between the two planets, conditions on the Sun can change drastically. Active regions may emerge or subside. Also, a coronal mass ejection that encounters Earth may miss Mars or may have a greater or lesser impact. These factor into the solar wind pressure incident at any given time.

[36] What should be similar between the two data sets is the distribution of solar wind pressure. Although the same events do not affect both Earth and Mars at high separation angles, the Sun should undergo similar numbers of events. That is, although the same ICME may not impact both Earth and Mars, Earth and Mars should experience transients from a similar number of ICMEs over the course of a year. Figure 6 is a histogram comparing the distribution of solar wind pressure inferred by the method above (gray bars) and scaled Wind data (dashed line). A lognormal distribution fit to the Wind data from 2 October 1997 to 31 December 1998 was performed and the parameters are given in Figure 6. p_{MGS} over the same time period is similar enough that we are confident in the method's ability to determine the relative solar wind pressure at Mars. We can therefore classify our data according to the solar wind pressure inferred for each orbital pass.

4.4. Response of Photoelectron Boundary

[37] D. Mitchell (private communication, 2000) has already shown that the photoelectron boundary (PEB) responds to P_{sw} as expected. Increased P_{sw} depresses the altitude of the PEB above regions without significant crustal magnetization. At Venus, when the incident ram pressure exceeds the ionospheric thermal pressure, the IMF permeates the ionosphere [*Luhmann et al.*, 1980]. When ionospheric pressure is sufficient to withstand P_{sw}, the ionopause was observed to fluctuate in response to P_{sw}. The martian ionosphere is usually in the overpressure regime [*Slavin and Holzer*, 1982].

[38] Because the PEB behaves as expected, the proxy for solar wind pressure developed for the mapping orbit is likely valid. They used a $\cos^2$ fit to the magnetic field at the near-400 km MGS mapping orbit to estimate P_{sw}. *Vennerstrom et al.* [2003] have also successfully used magnetic field in the MPR from mapping orbits as a proxy for solar wind pressure. Such fits are not possible with the premapping data described in this paper because of the range of spacecraft altitudes. However, its success lends credence to the method described here.

5. Response of the MPB

[39] Now that we have developed the proxy, we use it to determine the response of the solar wind interaction with Mars to changing solar wind pressure. Our focus is the position of the magnetic pileup boundary, which appears to be the obstacle for the solar wind protons [*Lundin et al.*, 1989; *Rosenbauer et al.*, 1989]. Although solar wind electrons and magnetic field appear to penetrate the MPB, model predictions of the magnetosheath fit best if the MPB is chosen to be the inner boundary for a gasdynamic model [*Spreiter and Stahara*, 1980].

[40] The response of the MPB position to solar wind pressure provides information about the nature of the obstacle Mars presents to the solar wind. An ionospheric obstacle to the solar wind is less responsive to P_{sw} than a magnetic obstacle. In a purely magnetic obstacle, an increase in solar wind pressure corresponds to a decrease in the subsolar magnetopause distance. Similarly, an increase in the solar wind pressure at Mars is expected to locally compress any crustal "magnetospheres." The extent to which this occurs is the subject of ongoing work.

[41] Phobos-2 had appropriate instrumentation to measure the dynamic pressure of the upstream solar wind. Through most of its mission, Phobos-2 was in a circular orbit near the equatorial plane at the distance of 9600 km from the center of Mars. In this phase, the spacecraft crossed the MPB in the tail. Increased solar wind pressure compresses the obstacle, yielding a smaller cavity in the tail [*Verigin et al.*, 1993]. They found the following relationship between the diameter of the tail and the solar wind pressure, $D^{-6} \propto P_{sw}$. We now look for the effects of solar wind dynamic pressure on the MPB position in the MGS data. To accommodate MPB crossings from many solar zenith angles, we invoke a mapping function to trace the MPB shape from the observation point to where the MPB crosses the terminator plane. We use the conic section fit to the average MPB position from *Vignes et al.* [2000]. (Figure 3 of *Vignes et al.* [2000] and Figure 2 of *Crider et al.* [2002] plot both the conic section fit and data in axisymmetric-cylindrical coordinates and as a function of solar zenith angle, respectively.) We call the result the "MPB mapped terminator distance" or $R_{term}(MPB)$. We plot $R_{term}(MPB)$ as a function of P_{sw} in Figure 7. A point is included for every MPB crossing in which the solar wind pressure was

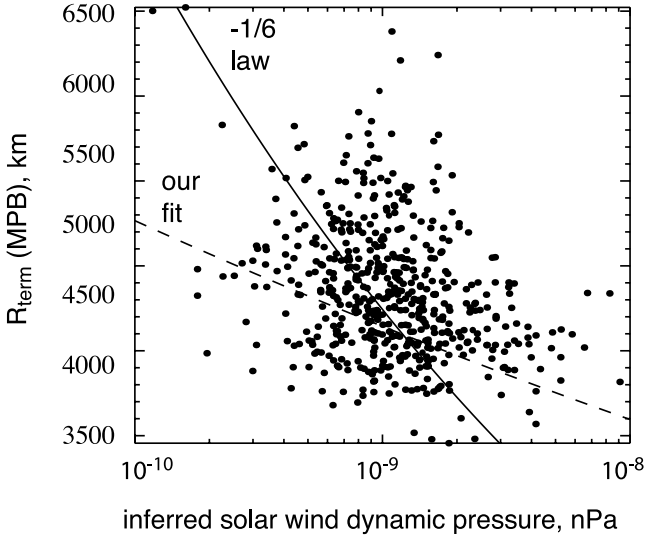

Figure 7. The mapped terminator distance of the MGS MPB crossings are plotted verses solar wind pressure. Power law fits (equation (4) and $p_{sw}^{-1/6}$) are superposed (dashed and solid lines, respectively).

available. Therefore, the other factors influencing the MPB position have not been extracted from the data in Figure 7. A power law fit is given by:

$$R_{term}(MPB) = 4644\,\mathrm{km}\,P_{sw}^{-0.0546}, \quad (4)$$

where P_{sw} is in nPa.

[42] Figure 8 is a histogram of the mapped terminator distance of the MPB for the data in Figure 7 separated into two groups of solar wind pressure: $P_{sw} \leq 1.1$ nPa and $P_{sw} > 1.1$ nPa. The high P_{sw} group is on average 181 km lower (or 13% of the MPB altitude) than the low P_{sw} group by best fit Gaussians to the groups. There is a 16% chance that these samples come from the same distribution.

[43] However, other factors are known to affect the position of the MPB. That is why the distribution about the mean is so large in Figure 8. In order to isolate the effects of P_{sw}, we next try to account for other factors involved in the determining the location of the MPB.

[44] Crustal magnetic fields are capable of locally diverting the flow. A hemispheric asymmetry is observed in the position of the MPB in which the MPB is further from the planet on average and more variable in the southern hemisphere in planet-fixed coordinates [*Crider et al.*, 2002]. This is the region where crustal magnetic sources are concentrated [*Connerney et al.*, 1999, 2001]. In order to discern other possible factors involved in the position of the MPB, we look only at crossings in the northern hemisphere of Mars, limiting the influence of crustal sources.

[45] Because the ion gyroradius is large compared with the size of the interaction region, there is a well-known asymmetry in the pick-up of new ions in the direction of the motional electric field of the solar wind [see, e.g., *Zhang et al.*, 1991; *Cable and Steinolfson*, 1995]. The electric field is in the $-\mathbf{v_{sw}} \times \mathbf{B_{IMF}}$ direction. A newly ionized ion will be accelerated in the direction of the apparent electric field direction. Roughly half of all ions created near the planet, those created in the "E−" hemisphere, will follow trajectories that intersect with the atmosphere before completing a gyration. These ions are deposited back into the atmosphere. The other half, which are accelerated away from the planet, are successfully picked up by the solar wind. For this reason, an asymmetry in the flow is expected in a coordinate system with the +z-axis aligned with the electric field direction. *Vennerstrom et al.* [2003] have detected this asymmetry in MGS mapping data.

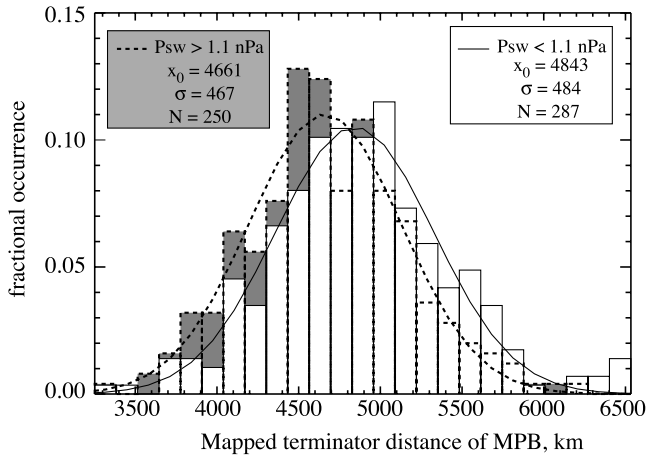

Figure 8. Histogram showing the mapped terminator distance of the MGS MPB crossings divided into high solar wind pressure and low solar wind pressure groups. Parameters for a Gaussian fit to each histogram are given.

[46] Next, we attempt to account for the contributions from the crustal magnetic fields and the pick-up ion asymmetry by selecting only MPB crossings that occur in the northern hemisphere in planetocentric coordinates and the E− hemisphere in IMF coordinates. (We could have used crossings in the E+ hemisphere instead; however, there were more crossings in the E− hemisphere.) We plot in Figure 9 the distribution of $R_{term}(MPB)$ for cases in which the solar wind dynamic pressure was less than 1.1 nPa and

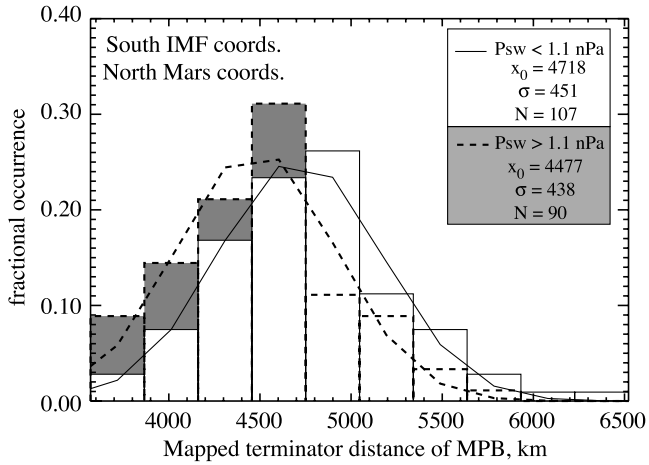

Figure 9. Histogram showing the mapped terminator distance of the MGS MPB crossings divided into high solar wind pressure and low solar wind pressure groups. Only MPB crossings from the northern hemisphere of Mars and from the E- hemisphere are used. Parameters for Gaussian best fits are given.

greater than 1.1 nPa. The average MPB position is 241 km lower in the high pressure group than in the low pressure group. There is only a 5% chance that these samples are from the same distribution.

[47] We sorted the data by several other groupings to see if there was another recognizable factor contributing to the position of the MPB. None was detected.

6. Conclusions

[48] Magnetic pressure is the dominant pressure term in the magnetic pileup region of Mars. It approximately balances the solar wind dynamic pressure. Therefore lacking other instrumentation to determine the solar wind pressure at Mars throughout the MGS mission, we find that we can use the magnetic field in the MPR as a reasonable proxy for the upstream solar wind dynamic pressure. We take the magnetic field measured in the MPR on the dayside of the planet at locations away from known crustal sources. We allow the pressure to fall off due to the angle of the incident flow to the surface normal. The resulting pressure is the inferred solar wind dynamic pressure.

[49] The method is validated in the following ways. First, using data from the mapping orbit of MGS, in which the spacecraft is fixed in a near-circular, near-polar orbit which skims the top of the ionosphere, *Vennerstrom et al.* [2003] established that the magnetic field magnitude in the MPR does follow the $\cos^2$ law. In mapping phase data, the altitude of the photoelectron boundary responds to the solar wind pressure in the appropriate fashion (D. Mitchell, private communication, 2000). Finally, we show that the inferred solar wind pressure has a distribution that is in good agreement with the measured solar wind pressure at Earth for the same time period. Therefore we find that the magnetic field pressure within the magnetic pileup region of Mars can be used as an effective proxy for upstream solar wind dynamic pressure at Mars.

[50] Increased solar wind pressure appears to compress the martian MPB. The position of the MPB is observed to move downwards when the solar wind pressure is high using MGS data. This agrees with observations in the martian tail from previous Phobos-2 data. The current study shows that the average mapped terminator position of the MPB can vary by ~250 km from low P_{sw} to high P_{sw}. (The average MPB altitude at the terminator is ~1350 km, for reference.) Our method of determining the upstream solar wind pressure by assuming magnetic pressure in the magnetic pileup region balances solar wind dynamic pressure appears to provide a decent proxy. Clearly, to fully understand the solar wind interaction with Mars, we need to include more comprehensive plasma instrumentation on future Mars orbiters.

[51] **Acknowledgments.** The authors thank A. Szabo and T. Narock for providing Wind data. This work was performed under NASA grants NAG5-11225 and NAG5-12235. TKB and AMK are partially supported by INTAS-ESA-55-00066 grant.

[52] Lou-Chuang Lee thanks Hector Perez-de-tejeda and another reviewer for their assistance in evaluating this paper.

References

Acuña, M. H., et al., Mars Observer magnetic fields investigation, *J. Geophys. Res.*, *97*, 7799–7814, 1992.

Acuña, M. H., et al., Magnetic field and plasma observations at Mars: Initial results of the Mars Global Surveyor mission, *Science*, *279*, 1676–1680, 1998.

Acuña, M. H., et al., Global distribution of crustal magnetization discovered by the Mars Global Surveyor MAG/ER experiment, *Science*, *284*, 790–793, 1999.

Acuña, M. H., et al., Magnetic field of Mars: Summary of results from the aerobraking and mapping orbits, *J. Geophys. Res.*, *106*, 23,403–23,417, 2001.

Albee, A. L., R. E. Arvidson, F. Pallucioni, and T. Thorpe, Overview of the Mars Global Surveyor mission, *J. Geophys. Res.*, *106*, 23,291–23,316, 2001.

Bertucci, C., et al., Magnetic field draping enhancement at the martian magnetic pileup boundary from Mars Global Surveyor observations, *Geophys. Res. Lett.*, *30*(2), 1099, doi:10.1029/2002GL015713, 2003.

Brain, D. A., The influence of crustal magnetic sources on the topology of the Martian magnetic environment, Ph.D. thesis, Univ. of Colo., Boulder, Colo., 2002.

Brain, D. A., et al., Observations of low-frequency electromagnetic plasma waves upstream from the Martian shock, *J. Geophys. Res.*, *107*(A6), 1076, doi:10.1029/2000JA000416, 2002.

Brain, D. A., F. Bagenal, M. H. Acuña, and J. E. P. Connerney, Martian magnetic morphology: Contributions from the solar wind and crust, *J. Geophys. Res.*, *108*(A12), 1424, doi:10.1029/2002JA009482, 2003.

Breus, T. K., E. M. Dubinin, A. M. Krymskii, R. Lundin, and J. G. Luhmann, The solar wind interaction with Mars: Consideration of Phobos 2 mission observations of an ion composition boundary on the dayside, *J. Geophys. Res.*, *96*, 11,165–11,174, 1991.

Cable, S., and R. S. Steinolfson, Three-dimensional MHD simulations of the interaction between Venus and the solar wind, *J. Geophys. Res.*, *100*, 21,645–21,658, 1995.

Chen, Y., P. A. Cloutier, D. H. Crider, C. Mazelle, and H. Rème, On the role of charge exchange in the formation of the Martian magnetic pileup boundary, *J. Geophys. Res.*, *106*, 29,387–29,400, 2001.

Cloutier, P. A., et al., Venus-like interaction of the solar wind with Mars, *Geophys. Res. Lett.*, *26*, 2685–2688, 1999.

Connerney, J. E. P., M. H. Acuna, P. J. Wasilewski, N. F. Ness, H. Reme, C. Mazelle, D. Vignes, R. P. Lin, D. L. Mitchell, and P. A. Cloutier, Magnetic lineations in the ancient crust of Mars, *Science*, *284*, 794–798, 1999.

Connerney, J. E. P., M. H. Acuña, P. J. Wasilewski, G. Kletetschka, N. F. Ness, H. Rème, R. P. Lin, and D. L. Mitchell, The global magnetic field of Mars and implications for crustal evolution, *Geophys. Res. Lett.*, *28*, 4015–4018, 2001.

Crider, D. H., The influence of crustal magnetism on the solar wind interaction with Mars: Recent observations, *Adv. Space Res.*, in press, 2003.

Crider, D. H., et al., Evidence of electron impact ionization in the magnetic pileup boundary of Mars, *Geophys. Res. Lett.*, *27*, 45–48, 2000.

Crider, D. H., et al., Magnetic field draping around Mars: Mars Global Surveyor results, *Adv. Space Res.*, *27*, 1831–1836, 2001.

Crider, D. H., et al., Observations of the latitude dependence of the location of the Martian magnetic pileup boundary, *Geophys. Res. Lett.*, *29*(8), 1170, doi:10.1029/2001GL013860, 2002.

Crider, D. H., D. A. Brain, M. Acuña, D. Vignes, C. Mazelle, and C. Bertucci, Mars Global Surveyor observations of solar wind magnetic field draping around Mars, ISSI, *Space Sci. Rev.*, in press, 2003.

Diodato, L., G. Moreno, C. Signorini, and K. W. Ogilvie, Long-term variations of the solar wind proton parameters, *J. Geophys. Res.*, *79*(34), 5095–5108, 1974.

Dubinin, E., K. Sauer, R. Lundin, O. Norberg, J. G. Trotignon, K. Schwingenschuh, M. Delva, and W. Riedler, Plasma characteristics of the boundary layer in the martian magnetosphere, *J. Geophys. Res.*, *101*, 27,061–27,075, 1996.

Krymskii, A. M., T. K. Breus, N. F. Ness, M. H. Acuna, J. E. P. Connerney, D. H. Crider, D. L. Mitchell, and S. J. Bauer, Structure of the magnetic field fluxes connected with crustal magnetization and topside ionosphere at Mars, *J. Geophys. Res.*, *107*(A9),1245, doi:10.1029/2001JA000239, 2002.

Luhmann, J. G., R. C. Elphic, C. T. Russell, J. D. Mihalov, and J. H. Wolfe, Observations of large-scale steady magnetic-fields in the dayside Venus ionosphere, *Geophys. Res. Lett.*, *7*, 917–920, 1980.

Lundin, R., A. Zakharov, R. Pellinen, H. Borg, B. Hultqvist, N. Pissarenko, E. M. Dubinin, S. W. Barabash, I. Liede, and H. Koskinen, First measurements of the ionospheric plasma escape from Mars, *Nature*, *341*, 609–612, 1989.

Lundin, R., et al., ASPERA/PHOBOS measurements of the ion outflow from the martian ionosphere, *Geophys. Res. Lett.*, *17*, 873–876, 1990.

Mitchell, D. L., R. P. Lin, H. Reme, D. H. Crider, P. A. Cloutier, J. E. P. Connerney, M. H. Acuna, and N. F. Ness, Oxygen Auger electrons observed in Mars' ionosphere, *Geophys. Res. Lett.*, *27*, 1871–1874, 2000.

Mitchell, D. L., R. P. Lin, C. Mazelle, H. Reme, P. A. Cloutier, J. E. P. Connerney, M. H. Acuna, and N. F. Ness, Probing Mars' crustal magnetic

field and ionosphere with the MGS Electron Reflectometer, *J. Geophys. Res.*, *106*, 23,418–23,427, 2001.

Øieroset, M., D. L. Mitchell, T. D. Phan, R. P. Lin, D. H. Crider, and M. H. Acuña, The magnetic field pile-up and density depletion in the Martian magnetosheath: A comparison with the plasma depletion layer upstream of the Earth's magnetopause, *Space Sci. Rev.*, in press, 2003.

Rosenbauer, H., et al., Ions of martian origin and plasma sheet in the martian magnetosphere: Initial results of the TAUS experiment, *Nature*, *341*, 612–614, 1989.

Schwingenschuh, K., et al., The Martian magnetic field environment: Induced or dominated by an intrinsic magnetic field?, *Adv. Space Res.*, *12*, 213–219, 1992.

Sheeley, N. R., and Y. M. Wang, Magnetic-field configurations associated with fast solar-wind, *Sol. Phys.*, *131*, 165–186, 1991.

Sibeck, D. G., R. E. Lopez, and E. C. Roelof, Solar-wind control of the magnetopause shape, location, and motion, *J. Geophys. Res.*, *96*, 5489–5495, 1991.

Slavin, J. A., and R. E. Holzer, The solar wind interaction with Mars revisited, *J. Geophys. Res.*, *87*, 10,285–10,296, 1982.

Slavin, J. A., R. C. Elphic, C. T. Russell, F. L. Scarf, J. H. Wolfe, J. D. Mihalov, D. S. Intriligator, L. H. Brace, H. A. Taylor, and R. E. Daniell, The solar wind interaction with Venus: Pioneer Venus observations of bow shock location and structure, *J. Geophys. Res.*, *85*, 7625–7641, 1980.

Slavin, J. A., K. Schwingenschuh, W. Riedler, and Y. Yeroshenko, The solar wind interaction with Mars: Mariner 4, Mars 2, Mars 3, Mars 5, and Phobos 2 observations of bow shock position and shape, *J. Geophys. Res.*, *96*, 11,235–11,241, 1991.

Spreiter, J. R., and S. S. Stahara, A new predictive model for determining solar wind-terrestrial planet interactions, *J. Geophys. Res.*, *85*, 6769–6777, 1980.

Spreiter, J. R., and S. S. Stahara, Computer modeling of the solar wind interaction with Venus and Mars, in *Venus and Mars: Atmospheres, Ionospheres, and Solar Wind Interactions*, *Geophys. Monogr. Ser.*, vol. 66, edited by J. G. Luhmann, M. Tatrallyay, and R. O. Pepin, pp. 345–383, AGU, Washington, D. C., 1992.

Trotignon, J. G., R. Grard, S. Barabash, R. Lundin, and E. Dubinin, Solar wind measurements near Mars and their implication in the Red Planet environment, *Planet. Space Sci.*, *44*, 117–127, 1996.

Vaisberg, O. L., D. S. Intriligator, and V. N. Smirnov, An empirical model of the Venusian outer environment. I - The shape of the dayside solar wind-atmosphere interface. II - The shape and location of the bow shock, *J. Geophys. Res.*, *85*, 7642–7654, 1980.

Vennerstrom, S., N. Olsen, M. Purucker, and M. Acuña, The magnetic field in the pile-up region at Mars and its variation with the solar wind, *Geophys. Res. Lett.*, *30*(7), 1369, doi:10.1029/2003GL016883, 2003.

Verigin, M. I., et al., The dependence of the Martian magnetopause shape and bow shock on solar wind dynamic pressure according to Phobos 2 TAUS ion spectrometer measurements, *J. Geophys. Res.*, *98*, 1303–1309, 1993.

Verigin, M., D. Vignes, D. Crider, J. Slavin, M. Acuña, G. Kotova, and A. Remizov, Martian obstacle and bow shock: Origins of boundaries anisotropy, *Adv. Space Res.*, *31*, in press, 2003.

Vignes, D., C. Mazelle, H. Rème, M. H. Acuña, J. E. P. Connerney, R. P. Lin, D. L. Mitchell, P. Cloutier, D. H. Crider, and N. F. Ness, The solar wind interaction with Mars: Locations and shapes of the bow shock and the magnetic pile-up boundary from the observations of the MAG/ER experiment onboard Mars Global Surveyor, *Geophys. Res. Lett.*, *27*, 49–52, 2000.

Vignes, D., M. H. Acuña, J. E. P. Connerney, D. H. Crider, H. Rème, and C. Mazelle, Factors controlling the location of the bow shock at Mars, *Geophys. Res. Lett.*, *29*(10), 1328, doi:10.1029/2001GL014513, 2002.

Zhang, T. L., J. G. Luhmann, and C. T. Russell, The magnetic barrier at Venus, *J. Geophys. Res.*, *96*, 11,145–11,153, 1991.

Zwan, B. J., and R. A. Wolf, Depletion of solar wind plasma near a planetary boundary, *J. Geophys. Res.*, *81*, 1636–1648, 1976.

M. Acuña, J. Slavin, and D. Vignes, NASA Goddard Space Flight Center, Mail Code 695, Greenbelt, MD 20771, USA. (mario.h.acuna@nasa.gov; james.a.slavin@nasa.gov; didier_vignes@hotmail.com)

T. K. Breus, Space Research Institute, Russian Academy of Sciences, Profsoyznaya 84/32, 117997 GSP-7, Moscow, Russia. (breus@space.ru)

D. Crider, 106 Driftwood Dr., Gibsonville, NC 27249, USA. (dcrider@lepvax.gsfc.nasa.gov)

A. M. Krymskii, Space Physics Department, Rostov State University, 5 Zorge Street, 344090 Rostov-on-Don, Russia. (amkrym@yahoo.com)

D. L. Mitchell, Space Sciences Laboratory, University of California, Berkeley, CA 94720, USA. (mitchell@ssl.berkeley.edu)

N. F. Ness, Bartol Research Institute, University of Delaware, Newark, DE 19716, USA. (nfness@udel.edu)